# Attainable Regions for Reaction with Separation

**Alberto Nisoli, Michael F. Malone, and Michael F. Doherty**
Dept. of Chemical Engineering, University of Massachusetts, Amherst, MA 01003

*The attainable region approach for reaction–mixing systems is combined with geometric methods for the feasibility of separations. The result is a systematic approach to identify the feasible compositions that can be achieved in processes combining simultaneous reaction, mixing, and separation. An activity-based formulation for both nonideal VLE and reaction-rate expressions is applied to develop hybrid reactor–separator models for the multiphase CSTR and PFR with simultaneous vapor removal. A reaction–separation vector is defined that satisfies the same geometric properties as the reaction vector. Therefore, the attainable region can be constructed following the existing procedure for reaction–mixing systems. This approach provides a method to generate feasible process alternatives. The technique is demonstrated on two nonideal ternary mixtures: the production of dimethyl ether by dehydration of methanol, and the production of methyl tert-butyl ether from isobutene and methanol. It is shown that for hybrid reaction–separation devices the entire composition space is not always attainable. In such cases, combining a hybrid device with traditional nonreactive separations is required to attain certain products.*

## Introduction

The synthesis of reactor networks has been studied using a variety of approaches, mostly based on optimization techniques. One approach considers fixed structures of reactors in which potential improvements can be made: Aris, in early pioneering work (1960a, b, c; 1961), applied dynamic programming to find the best temperature profiles and residence-time distributions in different reactors, by maximizing a profit function. Another approach does not assume a fixed reactor network, but determines the best reactor system for given operating conditions, such as the reactor temperature and pressure; for example, Kokossis and Floudas (1990) studied this problem by optimizing a superstructure of continuous stirred-tank reactors (CSTRs) in many possible configurations. A combined approach tries to optimize the reactor structure and operating conditions at the same time by solving a mixed-integer nonlinear programming problem: Balakrishna and Biegler (1993) considered simultaneous synthesis of reaction, energy, and separation systems, and Kokossis and Floudas (1994) applied the superstructure previously developed to nonisothermal systems.

The attainable-region approach addresses reactor network feasibility based on geometric properties and allows one to identify feasible, but not optimal reactor sequences for production of the desired product.

Correspondence concerning this article should be addressed to M. F. Malone.

The notion of an attainable region, first introduced by Horn (1964), has been extensively investigated by Hildebrandt, Glasser, and their coworkers for processes that include reaction and mixing (Feinberg and Hildebrandt, 1995; Glasser et al., 1987, 1992, 1994; Gordorr et al., 1994; Hildebrandt and Glasser, 1990; Hildebrandt et al., 1990). For a given system of reactions with given reaction kinetics, the attainable region is defined as the portion of concentration space that can be achieved from a given feed composition by any combination of reaction and mixing (Glasser et al., 1987). This attainable region is sometimes called the "kinetically attainable region" to distinguish it from the "thermodynamically attainable region," which is determined by equilibrium constraints (Shinnar and Feng, 1985).

To construct the attainable region in concentration space, simple steady-state models for the isothermal CSTR and plug-flow reactor (PFR) with constant volume are applied:

$$c - c_0 = \tau r(c) \tag{1}$$

and

$$\frac{dc}{d\tau} = r(c) \qquad c(0) = c_0, \tag{2}$$

where $r$ is the reaction vector, which is a function of the instantaneous concentration and the temperature as a parameter. The direction of $r$ is such that reaction changes the concentration vector $c$ in the same direction as the reaction vector, at each point on the trajectory.

The geometric properties of reaction and mixing determine the boundary of the attainable region:

- The reaction vector is collinear with the vector defined as the difference between the feed and exit concentrations for each point of the CSTR locus;
- The reaction vector is tangent to the curve that represents the PFR trajectory [a generic property of autonomous ordinary differential equations (ODEs), $\dot{x} = f(x)$, is that the trajectory through any point $x^*$ has a tangent that is collinear with the vector field $f(x)$ evaluated at $x^*$, $f(x^*)$].
- When two streams of composition $c_1$ and $c_2$, respectively, are mixed, the resultant lies on the straight line between $c_1$ and $c_2$ (lever rule).

The following necessary conditions for the attainable region are derived:

- The region is convex: given two achievable compositions, $c_1$ and $c_2$, every composition that lies on the line segment joining $c_1$ and $c_2$ belongs to the attainable region;
- No reaction vector points outward from the region on its boundary: at each point of the boundary the reaction vector points inward, is tangent, or is zero.
- In the complement of the attainable region no reaction vector when extended can intersect the attainable region.

The original formulation of the attainable region has also been applied to 3-D systems (Hildebrandt and Glasser, 1990; Godorr et al., 1994), to adiabatic systems (Hildebrandt et al., 1990; Glasser et al., 1992), and to more complex reactor systems (Glasser et al., 1994). Omtveit et al. (1994) gave a graphical representation of reactor–separator–recycle systems in concentration space, but they have not considered reaction and separation together. Recently, the feasible products for the vapor–liquid separation of homogeneous ternary mixtures in processes involving separation and mixing have been studied; the geometry of three configurations of two flash stages in parallel, in series, and in series with reflux is described (Jobson et al., 1995).

Geometric methods are also useful in studying the feasibility of separations. A common approach is the residue curve map: a topological analysis of the structure of residue curve maps can be used to determine feasible regions of operation (Foucher et al., 1991). Geometric methods have also been applied to determine which products may be obtained in nonreactive distillation (Wahnschafft et al., 1992; Fidkowski et al., 1993). Residue curve maps have also been extended to reactive distillation processes, for both equilibrium (Espinosa et al., 1995; Ung and Doherty, 1995a,b,c,d) and kinetically controlled (Venimadhavan et al., 1994) reactions.

The goal of this work is to combine a geometric approach to reactor synthesis with the geometric approach to feasibility of separation in order to find feasible process alternatives in systems with simultaneous reaction and separation. In the next section activity-based models for reactor–separators are derived in mole fraction space and used to define a unique reaction–separation vector. The approach is then applied to two reactive distillation processes.

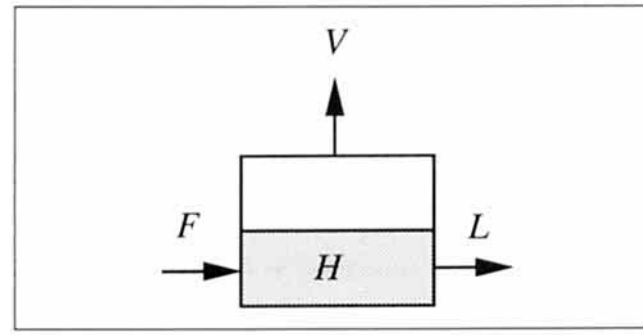


**Figure 1. CSTR with vapor removal.**

## CSTR with Vapor Removal

The two-phase CSTR reactor–separator consists of a flash separator with a simultaneous chemical reaction in the liquid phase, as shown in Figure 1. We consider a single chemical reaction and assume steady-state conditions and constant volume of the liquid phase. The reactor is isobaric and thus nonisothermal; the change in composition of the liquid phase due to reaction and separation causes the boiling temperature of the mixture to change.

We will use mole fractions and activity-based kinetic models in this development rather than concentrations for three reasons (Venimadhavan et al., 1994):

1. They are the basis for nonideal vapor–liquid equilibrium (VLE) in distillation problems.
2. When activity coefficients and mole fractions are used in the rate expression, they give a rate constant with units of reciprocal time regardless of the order of the reaction. This is convenient because it allows a universal definition of the dimensionless Damköhler number for all reaction orders.
3. The activity-based rate and (VLE) models give a consistent representation of both the phase equilibrium and the chemical equilibrium. Therefore, the long-time limit of the rate expression is guaranteed to agree with the reaction equilibrium model.

The overall material balance (Figure 1) can be written as

$$F - L - V + \nu_T r(x) H = 0, \tag{3}$$

where $r(x)$ is the reaction rate per mole of liquid mixture and has the units of reciprocal time, and $\nu_T$ is the algebraic sum of the stoichiometric coefficients. The streams $F$ and $L$ are assumed to be saturated liquids. The material balance for the $i$th component is:

$$Fx_{i,0} - Lx_i - Vy_i + \nu_i r(x) H = 0. \tag{4}$$

The liquid composition can be related to the vapor composition by any one of a number of VLE relationships. In this work we assume constant pressure and a temperature equal to the instantaneous boiling temperature of the liquid mixture. Hence the temperature of the system is determined by phase equilibrium, and the energy balance is needed only when we want to calculate the heating or cooling policy, which can be done separately. (A similar analysis can be carried out for systems with constant temperature and varying pressure.)

By eliminating $L$ from Eqs. 3 and 4, we obtain

$$x_i - x_{i,0} = \frac{V}{F}(x_i - y_i) + \frac{H}{F} r(x)(\nu_i - \nu_T x_i). \quad (5)$$

The molar liquid holdup is $H = \rho \upsilon$, where $\rho$ is the molar density of the liquid mixture and $\upsilon$ is the total volume of the liquid phase. It is useful to express the molar quantities $F$, $V$, and $\rho$ in terms of the corresponding mass quantities $F_m$, $V_m$, and $\rho_m$, leading to

$$x_i - x_{i,0} = \frac{V_m}{F_m}\frac{M(x_0)}{M(y)}(x_i - y_i) + \frac{\rho_m \upsilon}{F_m}\frac{M(x_0)}{M(x)} r(x)(\nu_i - \nu_T x_i), \quad (6)$$

where $M$ is the average molecular weight

$$M(x_0) = \sum_{i=1}^{N_C} M_i x_{i,0}, \quad (7)$$

Similar definitions apply to $M(x)$ and $M(y)$.

There are two reasons for using the mass variables $F_m$, $V_m$, and $\rho_m$ instead of molar quantities:

1. A common and reasonable assumption for the liquid phase is that the mass density can be considered approximately constant with respect to changes in the state of the system between inlet and outlet conditions.

2. We can introduce a parameter $\phi = V_m/F_m$ (the vapor fraction), which is defined over the interval 0 to 1. (If we used the same ratio in molar quantities, for a nonisomolar chemical reaction the upper bound of $\phi$ would be a function of conversion and it would not be possible to decouple the value of $\phi$ from the state of the system.)

We introduce a characteristic reaction time $(1/k_{f,\min})$ where $k_{f,\min}$ is a reference value of the forward rate constant, taken at the lowest temperature on the boiling surface (the lowest-boiling azeotrope or pure component in the system). The quantity $k_{f,\min}$ is used to define a Damköhler number $Da \equiv k_{f,\min}\rho_m \upsilon/F_m$, which is the ratio of a characteristic liquid residence time $(\rho_m \upsilon/F_m)$ to the characteristic reaction time $(1/k_{f,\min})$. No reaction occurs in the limit $Da \to 0$, and reaction equilibrium is achieved as $Da \to \infty$. For practical purposes reaction equilibrium is achieved for $Da \gg 1$. By incorporating the Damköhler number and the vapor fraction $\phi$ into Eq. 6 we obtain the final formulation:

$$x_i - x_{i,0} = \phi\frac{M(x_0)}{M(y)}(x_i - y_i) + Da\frac{M(x_0)}{M(x)}\frac{r(x)}{k_{f,\min}}(\nu_i - \nu_T x_i). \quad (8)$$

The difference between the composition vectors $x$ and $x_0$ is given in terms of a separation vector $(x - y)$ and a reaction vector $r(x)(\nu - \nu_T x)$. Given a value for $F$, a choice of $\phi$ sets all of the flows and $Da$ determines the reactor volume. These parameters can be chosen independently.

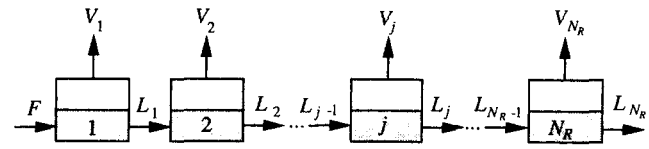


**Figure 2. Series of $N_R$ CSTRs with vapor removal.**

## PFR with Vapor Removal

We obtain the two-phase PFR model as the limit of a series of $N_R$ two-phase CSTRs when $N_R \to \infty$. The material balance for the $j$th reactor in the series (see Figure 2 and Eq. 8) is

$$x_{i,j} - x_{i,j-1} = \phi_j \frac{M(x_{j-1})}{M(y_j)}(x_{i,j} - y_{i,j}) + Da_j \frac{M(x_{j-1})}{M(x_j)}\frac{r(x_j)}{k_{f,\min}}(\nu_i - \nu_T x_{i,j}), \quad (9)$$

where the dimensionless parameters $\phi_j$ and $Da_j$ are defined as

$$\phi_j = \frac{V_{m,j}}{L_{m,j-1}} \quad (10)$$

$$Da_j = \frac{k_{f,\min}\rho_m \upsilon_j}{L_{m,j-1}}. \quad (11)$$

The values of $\phi_j$ and $Da_j$ are two independent parameters for each reactor. We make two assumptions for the series of CSTRs:

1. In each reactor the same fraction of the feed is vaporized, corresponding to

$$\phi_1 = \cdots = \phi_j = \cdots \phi_{N_R} \equiv \epsilon = \sum_{j=1}^{N_R} V_{m,j} / \sum_{j=1}^{N_R} L_{m,j-1}. \quad (12)$$

2. Every reactor has the same residence time, corresponding to

$$Da_1 = \cdots = Da_j = \cdots Da_{N_R} \equiv \delta = k_{f,\min}\rho_m \sum_{j=1}^{N_R} \upsilon_j / \sum_{j=1}^{N_R} L_{m,j-1}. \quad (13)$$

The quantities $\epsilon$ and $\delta$ are the same for each reactor, and once the total volume of the cascade and the total vapor rate are specified, they depend only on the number of reactors in the series. We can divide Eq. 9 by $Da_j$, leading to

$$\frac{x_{i,j} - x_{i,j-1}}{\frac{k_{f,\min}\rho_m}{L_{j-1}} A_j \Delta z_j} = \frac{\epsilon}{\delta}\frac{M(x_{j-1})}{M(y_j)}(x_{i,j} - y_{i,j}) + \frac{M(x_{j-1})}{M(x_j)}\frac{r(x_j)}{k_{f,\min}}(\nu_i - \nu_T x_{i,j}), \quad (14)$$

where $A_j \Delta z_j = v_j$, $A_j$ is the cross-sectional area and $\Delta z_j$ is the length of the $j$th reactor. The values of $\epsilon$ and $\delta$ are finite quantities for finite $N_R$ and they determine all the flows and all the reactor volumes in the cascade. When $N_R \to \infty$, $\epsilon$ and $\delta \to 0$ ($\sum_{j=1}^{N_R} L_{m,j-1} \to \infty$ when $N_R \to \infty$): the volume of each reactor and the quantity of vapor removed from each individual reactor become infinitesimally small. However, the ratio $\epsilon/\delta$ is finite since the quantity $\sum_{j=1}^{N_R} L_{m,j-1}$ cancels. We can express that ratio in terms of overall system parameters $\phi$ and $Da$:

$$\frac{\epsilon}{\delta} = \frac{\sum_{j=1}^{N_R} V_{m,j}}{k_{f,\min}\, \rho_m \sum_{j=1}^{N_R} v_j} = \frac{\sum_{j=1}^{N_R} V_{m,j}/F_m}{k_{f,\min}\, \rho_m \sum_{j=1}^{N_R} v_j/F_m} = \frac{\phi}{Da} \tag{15}$$

$$\phi = \frac{1}{F_m} \sum_{j=1}^{N_R} V_{m,j} \tag{16}$$

$$Da = \frac{k_{f,\min}\, \rho_m}{F_m} \sum_{j=1}^{N_R} v_j. \tag{17}$$

The parameter $\phi$ represents the total fraction of the inlet liquid flow rate that is vaporized in the cascade and depends on the heating policy; $Da$ represents the ratio of a characteristic residence time of the cascade of CSTRs to the characteristic reaction time.

The PFR behavior is found by taking the limit of Eq. 14 as $\Delta z_j \to 0$ ($N_R \to \infty$), giving:

$$\frac{dx_i}{d\zeta} = \frac{\phi}{Da} \frac{M(x)}{M(y)} (x_i - y_i) + \frac{r(x)}{k_{f,\min}} (\nu_i - \nu_T x_i) \tag{18}$$

where

$$d\zeta \equiv \frac{k_{k,\min}\, \rho_m}{L_m(z)} A(z)\, dz. \tag{19}$$

In the limit $N_R \to \infty$ the two dimensionless parameters $\phi$ and $Da$, defined in Eqs. 16 and 17, become:

$$\phi = \frac{1}{F_m} \int_0^l \bar{V}_m(z)\, dz \tag{20}$$

$$Da = \frac{k_{f,\min}\, \rho_m}{F_m} \int_0^l A(z)\, dz, \tag{21}$$

where $z$ is the distance along the reactor, $l$ is the length of the reactor, and $\bar{V}_m$ is the mass vaporization rate per unit length.

In order to express the CSTR locus and the PFR trajectory in terms of the same reaction–separation vector, Eq. 18 is multiplied by the ratio $M(x_0)/M(x)$. Since the ratio of molecular weights is strictly positive, it is possible to rescale the dimensionless time in the system of ODEs defined by Eq. 18, which is equivalent to

$$\frac{dx_i}{d\eta} = \frac{\phi}{Da} \frac{M(x_0)}{M(y)} (x_i - y_i) + \frac{M(x_0)}{M(x)} \frac{r(x)}{k_{f,\min}} (\nu_i - \nu_T x_i), \tag{22}$$

where

$$d\eta \equiv \frac{M(x)}{M(x_0)} d\zeta. \tag{23}$$

Since Eqs. 18 and 22 are autonomous their trajectories are identical. Once the parameters $\phi$ and $Da$ are set, they determine the stopping condition for the independent variables in Eqs. 18 and 22 (see the Appendix).

An application of this sort of reaction–separation model is the polymerization of nylon 6,6 in which a flowing-film model is used to design continuous-film polymerizers (e.g., Taylor, 1944; Jaswal et al., 1975; Pinney, 1976; Steppan et al., 1989, 1990).

## The Reaction–Separation Vector

The reaction–separation vector is defined as

$$\boldsymbol{R}(x, y) = \frac{\phi}{Da} \frac{M(x_0)}{M(y)} (x - y) + \frac{M(x_0)}{M(x)} \frac{r(x)}{k_{f,\min}} (\nu - \nu_T x). \tag{24}$$

It is possible to put Eqs. 8 and 22 in the same form as Eqs. 1 and 2 if we replace the reaction vector in concentration space with the reaction–separation vector in composition space:

$$x - x_0 = Da\boldsymbol{R}(x, y) \tag{25}$$

$$\frac{dx}{d\eta} = \boldsymbol{R}(x, y) \qquad x(0) = x_0. \tag{26}$$

Therefore, the same procedure to construct the attainable region for systems with reaction and mixing only (Glasser et al., 1987) can also be followed here for systems including separation. The procedure involves the following steps:

- Construct the plug-flow trajectory and the CSTR locus from the feed point. The curves are parameterized by the Damköhler number. The CSTR locus is found by solving Eq. 25, using a parameter continuation method in the Damköhler number, which is varied from zero to approximately 100 (this value is typically large enough to ensure a close approach to reaction equilibrium). For reaction with multiple steady states an arc-length continuation should be used. We also assume that the system does not exhibit isolated solutions (an arc-length continuation does not find isolated solutions). The PFR trajectory is calculated by solving the ODE system defined by Eq. 26.
- Construct a convex hull.
- If there exists a reaction–separation vector pointing outward, extend the hull by using a PFR.
- Repeat the previous steps until no reaction–separation vectors point out of the region; this region will be convex and it is the attainable region.

## Example: Synthesis of Dimethyl Ether

Dimethyl ether (DME), an important material in the areas of aerosols, refrigerants, and solvents, can be produced by

catalytic dehydration of methanol using alumina (Brake, 1986):

$$2CH_3OH \Leftrightarrow H_2O + CH_3OCH_3 \tag{27}$$

The stoichiometric coefficients are $\nu_1 = 1$, $\nu_2 = -2$, $\nu_3 = 1$, where the numbers 1, 2 and 3 indicate water, methanol, and DME, respectively. Therefore, $\nu_T = 0$. We have analyzed this mixture at a pressure of 15 atm (at this pressure cooling water can be used to condense DME). The system is nonideal, and although it has no azeotropes, it does have an immiscible region between water and DME, which shrinks as the pressure increases (i.e., as the boiling temperature of the mixture increases). We assume a pure methanol feed. As we will show later, all the reactor profiles stay above the chemical equilibrium curve, and this curve does not cross the liquid–liquid region at 15 atm (Figure 3). Therefore, the models previously developed for the two-phase CSTR and PFR can be applied. We use the NRTL model for the activity coefficients and introduce the Poynting correction for the liquid phase and the second virial coefficient for the vapor phase, which is considered to be an ideal mixture of imperfect gases (at reduced pressures up to $\sim 0.7$ pure liquids can generally be treated as incompressible and in the vapor phase the volume of mixing is negligible). With these assumptions, the VLE relation becomes:

$$Py_i \exp\left(\frac{B_i(T)(P - P_i^{sat})}{RT}\right) = P_i^{sat}\gamma_i x_i \exp\left(\frac{v_i^{0L}(P - P_i^{sat})}{RT}\right), \tag{28}$$

where $B_i(T)$ is the second virial coefficient and $v_i^{0L}$ is the liquid molar volume for the $i$th component. The data and correlations are given in Table 1. Where the mixture contains mostly water at 15 atm operating pressure, the boiling temperatures are in the range 335–470 K, which is above the critical temperature of DME ($T_c = 400$ K). However, since the reduced temperature of DME is far below 1.8, it can still be treated as a vapor (Prausnitz et al., 1980), and Eq. 28 can be used to represent the VLE.

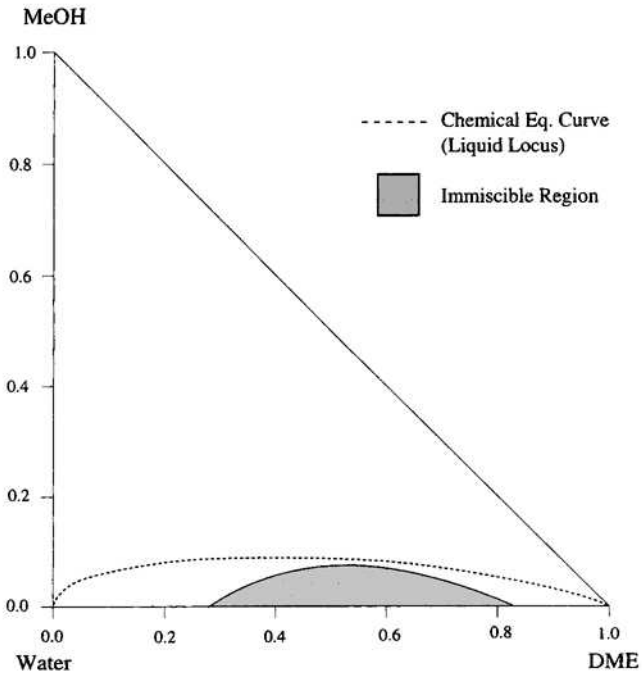


**Figure 3. DME system: immiscible region at 15 atm.**

The expression for the pseudohomogeneous reaction rate in the activity-based model is

$$r = k_f\left(x_2^2\gamma_2^2 - \frac{1}{K}x_1\gamma_1 x_3\gamma_3\right). \tag{29}$$

The equilibrium constant is represented by

$$K = \exp\left(-\frac{\Delta G^0}{RT}\right). \tag{30}$$

Based on the heats and free energies of formation (Reid et al., 1987) and on thermodynamic correlations (Modell and Reid, 1983), an expression for $\Delta G^0$ for the liquid phase reaction was obtained. In the range of operating temperatures we find a linear correlation for $\Delta G^0$:

$$\Delta G^0 = -2.4634 - 1.5167 \times 10^{-3} T, \tag{31}$$

where $\Delta G^0$ is in kcal/mol and $T$ is in Kelvin. The value of $K$ varies between 87 ($T = 335$ K) and 30 ($T = 470$ K).

We take $k_f$ to be independent of temperature in this range of boiling points and examine the effects of its magnitude by variation of $Da$.

To construct the attainable region we consider all combinations of the parameters $\phi$ and $Da$. When $\phi = 0$, no vaporization takes place. When $\phi = 1$, Eq. 22 is equivalent to a model for batch-reactive distillation (Venimadhavan et al., 1994) in which the liquid holdup is completely evaporated. Therefore, the case $\phi = 1$ gives the residue-curve map as a function of the Damköhler number.

To construct the attainable region we find the CSTR locus and the PFR trajectory. Since the mixture has three components, the CSTR locus and the PFR trajectory are found by solving a system of two algebraic equations (Eq. 8 for $i = 1, 2$) and two ODEs (Eq. 22 for $i = 1, 2$), respectively. We assume a feed composition of pure methanol. The Damköhler number is set equal to a large value ($\sim$ 100), since this enlarges the region the most: the composition profiles for smaller values of $Da$ are all contained in the envelope defined by the profiles at high $Da$. First we draw the CSTR locus and the PFR trajectory in the liquid phase for different values of the vapor fraction $\phi$ (Figures 4a to 4c). When $\phi = 0$, the temperature of the mixture is at the boiling point, but no vapor is removed; for $\phi = 0.5$, half of the feed is vaporized, and for $\phi = 1$, all of the feed is vaporized. When $\phi = 0$, the CSTR locus and the PFR trajectory coincide and the attainable region is just the straight line connecting $a$ and $b$ ($b$ is a point infinitesimally close to the chemical equilibrium curve. It lies on that curve only in the limit $Da \to \infty$). In fact for $\phi = 0$ there is a linear relationship between $x_3$ and $x_2$ due to stoichiometry, and which is independent of the reactor type (the same relationship holds for the vapor compositions when $\phi = 1$).

**Table 1. Vapor–Liquid Equilibrium Data for the DME Example**

Antoine Equation

$$\ln P_i^{sat} = A_i + \frac{B_i}{T + C_i}$$

$P_i^{sat}$[Pa], $T$[K]

Liquid Molar Volumes and Constants for the Antoine Equation

| Component | $v_i^{0L}$ [m³/mol] | $A_i$ | $B_i$ | $C_i$ |
|---|---|---|---|---|
| (1) Water | $18.05\times10^{-6}$ | 23.2256 | −3,835.18 | −45.343 |
| (2) Methanol | $40.51\times10^{-6}$ | 23.49989 | −3,643.31362 | −33.434 |
| (3) DME | $69.07\times10^{-6}$ | 21.2303 | −2,164.85 | −25.344 |

Second Virial Coefficient Equation

$$B_i(T) = A_i + \frac{B_i}{T} + \frac{C_i}{T^3} + \frac{D_i}{T^8} + \frac{E_i}{T^9}$$

$B_i(T)$ [m³/mol]

| Component | $A_i$ | $B_i$ | $C_i$ | $D_i$ | $E_i$ |
|---|---|---|---|---|---|
| (1) Water | $-2.3040\times10^{-5}$ | $2.6860\times10^{-2}$ | $-2.8170\times10^{4}$ | $3.3408\times10^{17}$ | $-1.3837\times10^{20}$ |
| (2) Methanol | $-6.4000\times10^{-4}$ | $6.2000\times10^{-1}$ | $-1.0710\times10^{5}$ | $7.7160\times10^{17}$ | $-2.1974\times10^{20}$ |
| (3) DME | $-1.0830\times10^{-4}$ | $-1.0440\times10^{-1}$ | $-5.6800\times10^{3}$ | $-4.0880\times10^{15}$ | $6.7440\times10^{17}$ |

NRTL Equation

$$\ln\gamma_i = \frac{\sum_{j=1}^{N_c}\tau_{j,i}G_{j,i}x_j}{\sum_{l=1}^{N_c}G_{l,i}x_l} + \sum_{j=1}^{N_c}\frac{x_jG_{i,j}}{\sum_{l=1}^{N_c}G_{l,j}x_l}\left(\tau_{i,j} - \frac{\sum_{n=1}^{N_c}x_n\tau_{n,j}G_{n,j}}{\sum_{l=1}^{N_c}G_{l,j}x_l}\right)$$

$$\tau_{j,i} = \frac{A_{j,i}}{RT} \qquad G_{j,i} = \exp(-\alpha_{j,i}\tau_{j,i})$$

$A_{j,i}$ [cal/mol]

Binary Interaction Parameters for the NRTL Equation

| | | |
|---|---|---|
| $A_{1,1} = 0.0$ | $A_{1,2} = 845.2062$ | $A_{1,3} = 792.7342$ |
| $A_{2,1} = -253.8802$ | $A_{2,2} = 0$ | $A_{2,3} = -19.66$ |
| $A_{3,1} = 1{,}203.776$ | $A_{3,2} = 794.144$ | $A_{3,3} = 0.0$ |
| $\alpha_{1,2} = 0.2994$ | $\alpha_{1,3} = 0.3$ | $\alpha_{2,3} = 0.3$ |

As we remove vapor, the value of $\phi$ increases, the PFR trajectory starts following the chemical equilibrium curve toward the water vertex, and the CSTR locus moves away from the DME vertex because the liquid phase becomes leaner in the lightest component (DME) and richer in the heaviest component (water). When $\phi = 1$, the PFR trajectory reaches the pure-water vertex (the same as a residue curve). The boundaries of the convex hull of feasible compositions in the liquid phase (Figure 4d) are the CSTR locus for $\phi = 0$, the methanol–water edge of the triangle, and the mixing line joining the point $b$ and the pure-water vertex.

Figure 5a to 5c show the corresponding vapor compositions for the three values of $\phi$. DME is very volatile, so the liquid phase gets enriched in water as the vapor phase gets enriched in DME. If an analogous procedure is followed for the vapor phase, it leads to the convex hull in Figure 5d. Since the convex hull for the vapor phase contains the convex hull for the liquid phase, it represents the attainable region.

An important way of enlarging the attainable region is to allow for condensation of the vapor stream(s) leaving the reactor(s). In this case, the entire composition space, that is, all of the triangle, becomes attainable. In fact we can imagine condensing the vapor at point $c$ (Figure 5b) and starting another vapor–liquid reactor with a feed composition corresponding to this point. The corresponding flow sheet is shown in Figure 6. The liquid stream leaving the new reactor will be richer in water, while the vapor stream will be richer in DME, and the point $d$ in Figure 5d will get closer to the pure DME vertex. If we repeat the procedure a few times, the reactor vapor product composition will essentially coincide with the pure DME vertex; therefore, all the composition space is attainable. Since every composition is attainable, the assumption we have made about the kinetics ($k_f = k_{f,\min}$) does not affect the final result. Changing this assumption will only change the way the CSTR loci and PFR trajectories approach the equilibrium curve.

Pure DME can be produced by using a reactive distillation column fed with pure methanol. Our analysis, carried out with multiphase reactors, leads to the same conclusion. This conclusion might be obvious, but it does not apply to other systems, such as the MTBE system. The attainable region approach allows us to prove that pure DME can be obtained when reaction and separation occur simultaneously. From a practical viewpoint the flowsheet we have shown in Figure 6 can be realized in a more efficient way by using a reactive distillation column where the flows are countercurrently contacted.

## Example: Synthesis of Methyl *tert*-Butyl Ether

Methyl *tert*-butyl ether can be made by reacting isobutene and methanol in the liquid phase at temperatures in the range

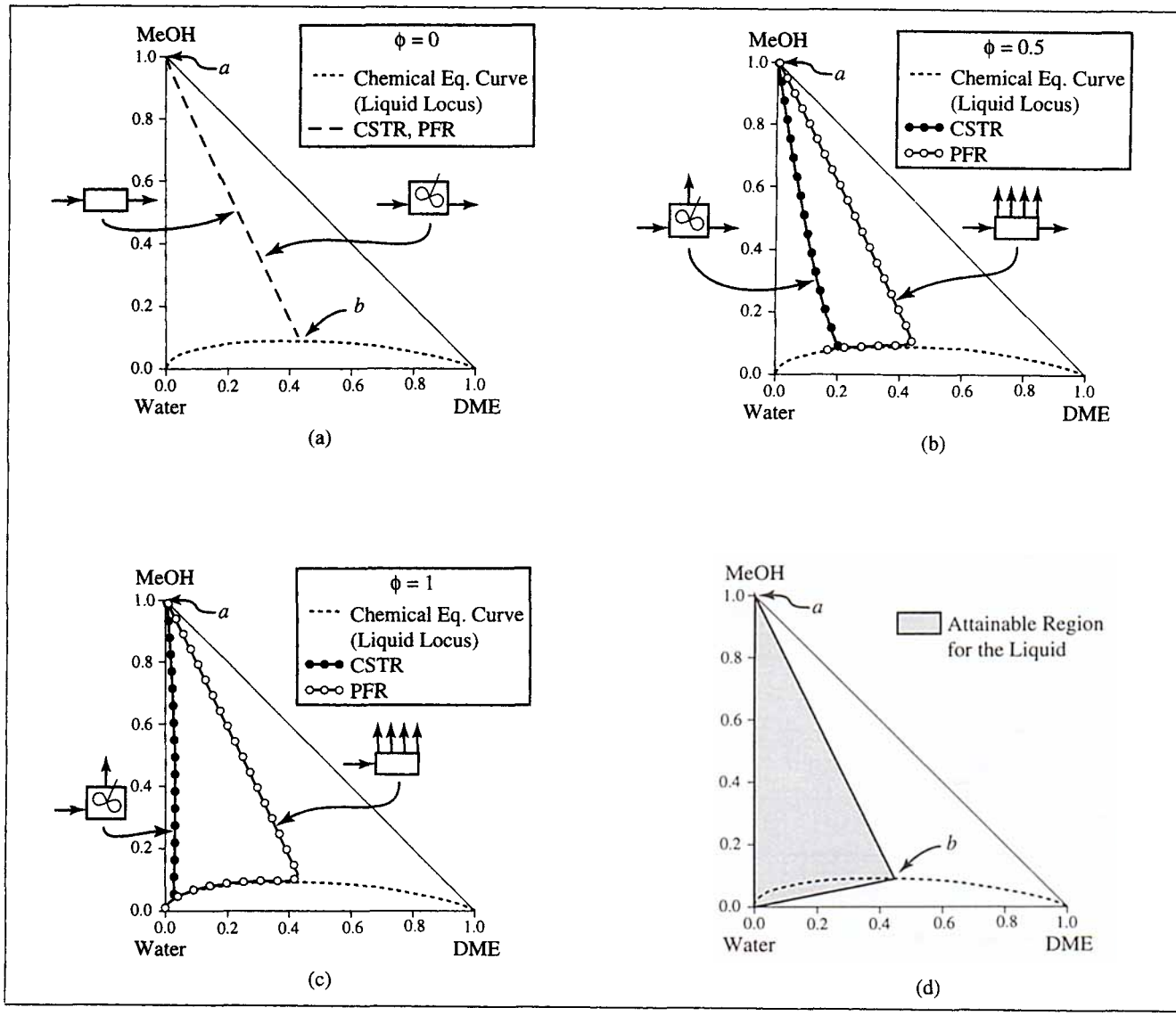


**Figure 4. DME system at 15 atm: reactor compositions and attainable region for the liquid.**

40 to 100°C, using an acid catalyst such as sulfuric acid (Al-Jarallah et al., 1988), or an ion-exchange resin (Rehfinger et al., 1990; Sundmacher and Hoffmann, 1992). The principal reaction is

$$i\text{-}C_4H_8 + CH_3OH \Leftrightarrow CH_3OC(CH_3)_3. \qquad (32)$$

The stoichiometric coefficients are $\nu_1 = -1$, $\nu_2 = -1$, $\nu_3 = 1$, where the numbers 1, 2 and 3 indicate isobutene, methanol, and MTBE, respectively. Therefore $\nu_T = -1$. The vapor–liquid equilibrium for this mixture is strongly non-ideal; it exhibits two minimum-boiling binary azeotropes over a wide range of pressures, one between isobutene and methanol, the other between methanol and MTBE. The two azeotropes give rise to a distillation boundary in the residue curve map for the nonreactive mixture (shown in Figure 7a at a pressure of 8 atm): a nonreactive distillation operated in the composition space below the boundary allows us to produce pure MTBE (as the bottom product), but the recovery of MTBE is limited. Figure 7b shows the corresponding residue curve map for the reactive system with chemical reaction essentially at equilibrium. The change in the topological features of the two residue curve maps has been treated in detail by Venimadhavan et al. (1994). The Wilson model is used to represent the activity coefficients and the Antoine equation is used for computing the pure component vapor pressures. A pressure of 8 atm was chosen, according to the experimental data of Al-Jarallah et al. (1988). At this pressure the gas phase can be considered ideal, so the VLE relation becomes

$$Py_i = P_i^{\text{sat}}\gamma_i x_i. \qquad (33)$$

An expression for the reaction rate in an activity-based model with sulfuric acid catalyst is (Venimadhavan et al., 1994)

$$r = k_f\left(x_1\gamma_1 x_2\gamma_2 - \frac{1}{K}x_3\gamma_3\right). \qquad (34)$$

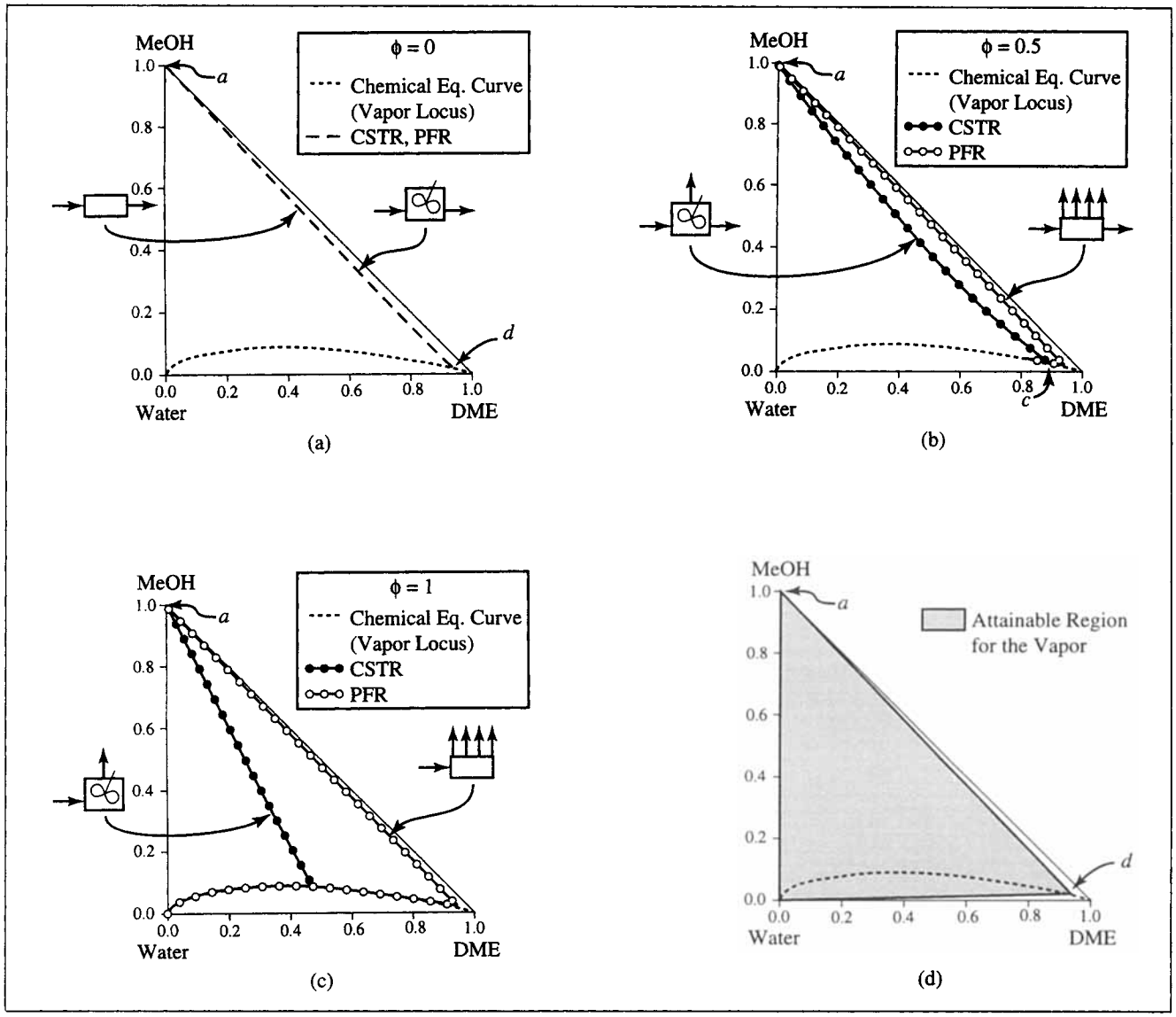


**Figure 5. DME system at 15 atm: reactor compositions and attainable region for the vapor.**

The temperature dependencies of the forward reaction-rate constant $k_f$ and the thermodynamic equilibrium constant $K$ are given by a linear least-squares fit (Venimadhavan et al., 1994) of the experimental data (Al-Jarallah et al., 1988):

$$k_f = 74.40e^{-3,187.0/T} \tag{35}$$

$$\ln(K) = \frac{6820.0}{T} - 16.33, \tag{36}$$

where the temperature $T$ is in K and $k_f$ has units of inverse minutes.

The data and correlations are given in Table 2. At the operating pressure, the lowest boiling point is the azeotrope between isobutene and methanol, with a composition of 6.7 mol % methanol at 60.2°C. The value of $k_{f,\min}$ at this temperature is 0.0052 $\min^{-1}$.

We start from an equimolar feed ($x_{1,0} = x_{2,0} = 0.5$). For feeds on the convex side of the chemical equilibrium curve, unlike the DME example, the profiles calculated for high $Da$ do not extend the region the most. First, we compute the attainable region for high $Da$, and we show that it is smaller than the whole composition space. Using this result as a basis, we will then examine the effects of low $Da$.

The attainable region for high $Da$ is constructed using the same procedure applied previously for the DME system. A value of $Da = 50$ is high enough for a close approach to the chemical equilibrium curve. The PFR trajectories and CSTR loci are shown in Figure 8a to 8c and Figure 9a to 9c for the liquid and the vapor phase, respectively. The profiles are plotted for three different values of the vapor fraction, $\phi = 0$, $\phi = 0.5$, and $\phi = 1$. The point $a$ represents the feed composition. Again we can see that the region can be extended by separation ($\phi > 0$). The CSTR locus moves from point $b$ (Figure 8a) to point $c$ (Figure 8c) as the vapor rate approaches the feed rate ($\phi \to 1$). The convex hull for the liquid is represented by the area between the segment $a-b$ and the equilibrium curve in Figure 8d.

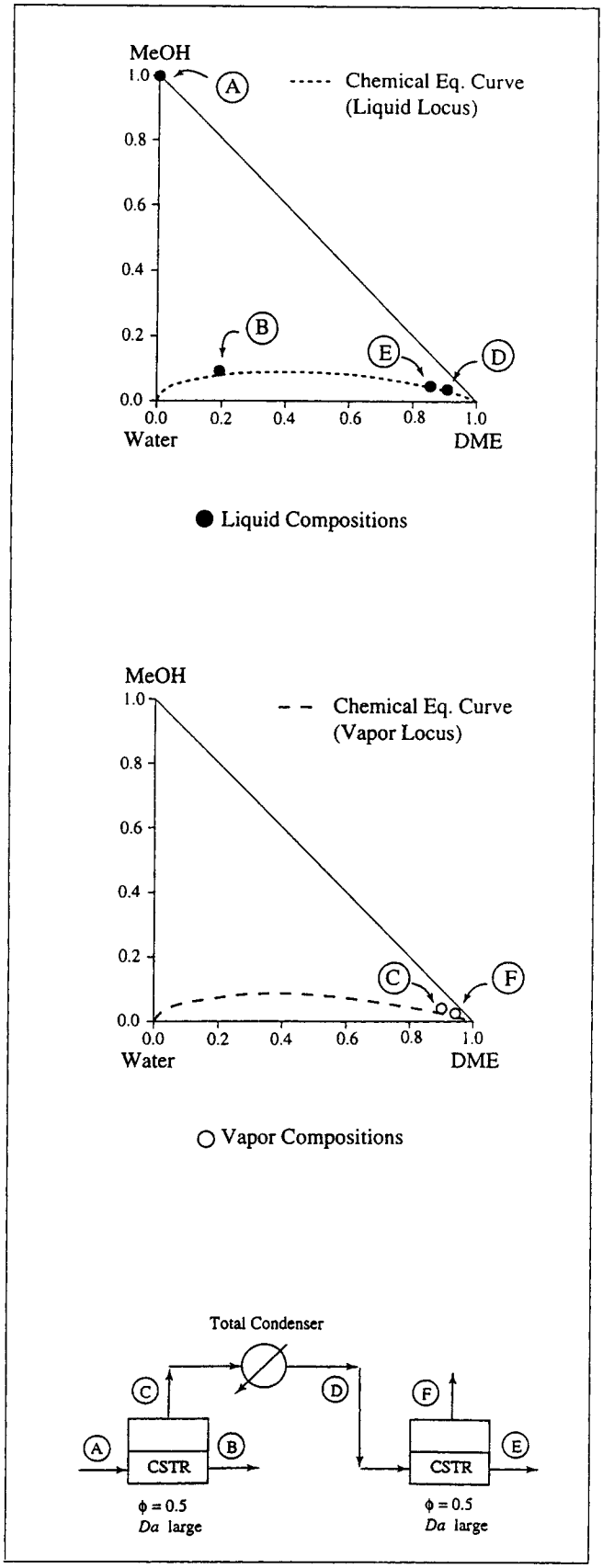


**Figure 6. DME system at 15 atm: example of flowsheet with stream compositions shown on triangular diagrams.**

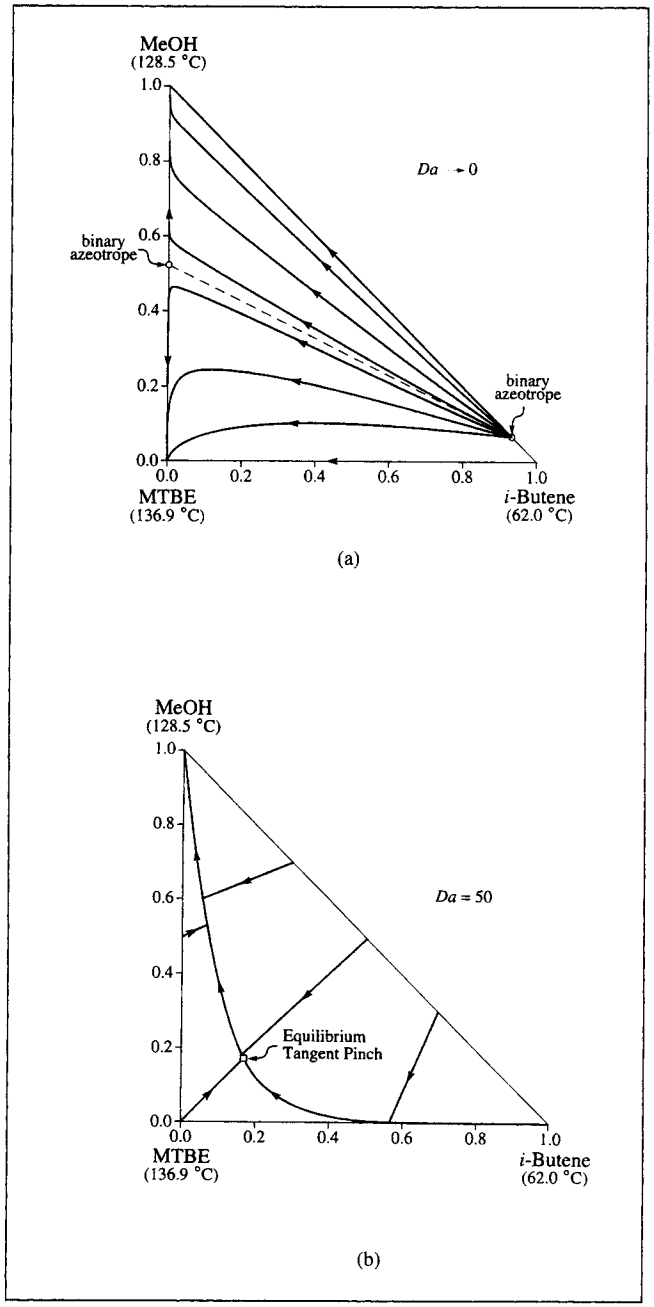


**Figure 7. Residue curve maps for the MTBE system at 8 atm pressure: (a) $Da \to 0$; (b) $Da = 50$; the dashed line in (a) represents the distillation boundary.**

Figure 9d shows the corresponding convex hull for the vapor, defined by points $a-f-e-g$-pure methanol. The points $e$ and $f$ are the vapor compositions in equilibrium with the liquid compositions $b$ and $a$, respectively. Two mixing lines (one between $e$ and $f$, and the other between $g$ and the methanol vertex) are drawn in order to make the region convex. If we condense the vapor at point $f$, we can construct the attainable region for the liquid phase with $f$ as the feed point, that is, the area $f-h-b$-pure methanol$-a-f$ (Figure 8d). After a few steps, the resultant attainable region for the

**Table 2. Vapor–Liquid Equilibrium Data for the MTBE Example**

Antoine Equation

$$\ln P_i^{sat} = A_i + \frac{B_i}{T + C_i}$$

$P_i^{sat}$[Pa], $T$[K]

Liquid Molar Volumes and Constants for the Antoine Equation

| Component | $\nu_i^{0L}$ | $A_i$ | $B_i$ | $C_i$ |
|---|---|---|---|---|
| (1) Isobutene | $93.33\times10^{-6}$ | 20.64556 | −2,125.74886 | −33.160 |
| (2) Methanol | $44.44\times10^{-6}$ | 23.49989 | −3,643.31362 | −33.434 |
| (3) MTBE | $118.8\times10^{-6}$ | 20.71616 | −2,571.58460 | −48.406 |

Wilson Equation

$$\ln \gamma_i = 1 - \ln\left(\sum_{j=1}^{N_c} x_j \Lambda_{i,j}\right) - \sum_{k=1}^{N_c} \frac{x_k \Lambda_{k,i}}{\sum_{j=1}^{N_c} x_j \Lambda_{k,j}}$$

$$\Lambda_{i,j} = \frac{\nu_i^{0L}}{\nu_j^{0L}} \exp\left(-\frac{A_{i,j}}{RT}\right)$$

$\nu_i^{0L}$ [m$^3$/mol], $A_{i,j}$[cal/mol]

Binary Interaction Parameters for the Wilson Equation

| | | |
|---|---|---|
| $A_{1,1} = 0.0$ | $A_{1,2} = 169.9953$ | $A_{1,3} = -60.1085$ |
| $A_{2,1} = 2{,}576.8532$ | $A_{2,2} = 0.0$ | $A_{2,3} = 1.483.2478$ |
| $A_{3,1} = 271.5669$ | $A_{3,2} = -406.3902$ | $A_{3,3} = 0.0$ |

MTBE system is given in Figure 10a. Therefore pure MTBE cannot be achieved from a hybrid reactor–separator system.

If we now consider the profiles for very small values of *Da*, the entire composition space becomes attainable, as shown in Figure 10b. The line connecting *a* and *b* represents a reactor (CSTR or PFR) with high *Da* and no separation ($\phi = 0$). The reactor trajectory crosses the distillation boundary. The profile from point *b* to the MTBE vertex corresponds to the residue curve for the nonreactive system ($\phi = 1$, $Da \to 0$). Hence, if we use separate reaction and separation steps, the entire composition space is also attainable.

In this case, the value of the attainable-region approach is that it tells us that we cannot reach pure MTBE using either reaction alone *or* reaction and separation simultaneously. The only two feasible flow sheets consist of a reactor followed by a separator (Figure 11a) or a reactor–separator unit followed by a separation system (Figure 11b: the reactor–separator is represented by the reactive section of the reactive distillation column). In the conventional process (Figure 11a) a recycle is needed: after the inerts removal the mixture still contains a large amount of MTBE, due to the presence of the distillation boundary. At this stage a design and cost estimate must be performed in order to determine which is the best alternative. Both alternatives are used in industrial practice (Smith,

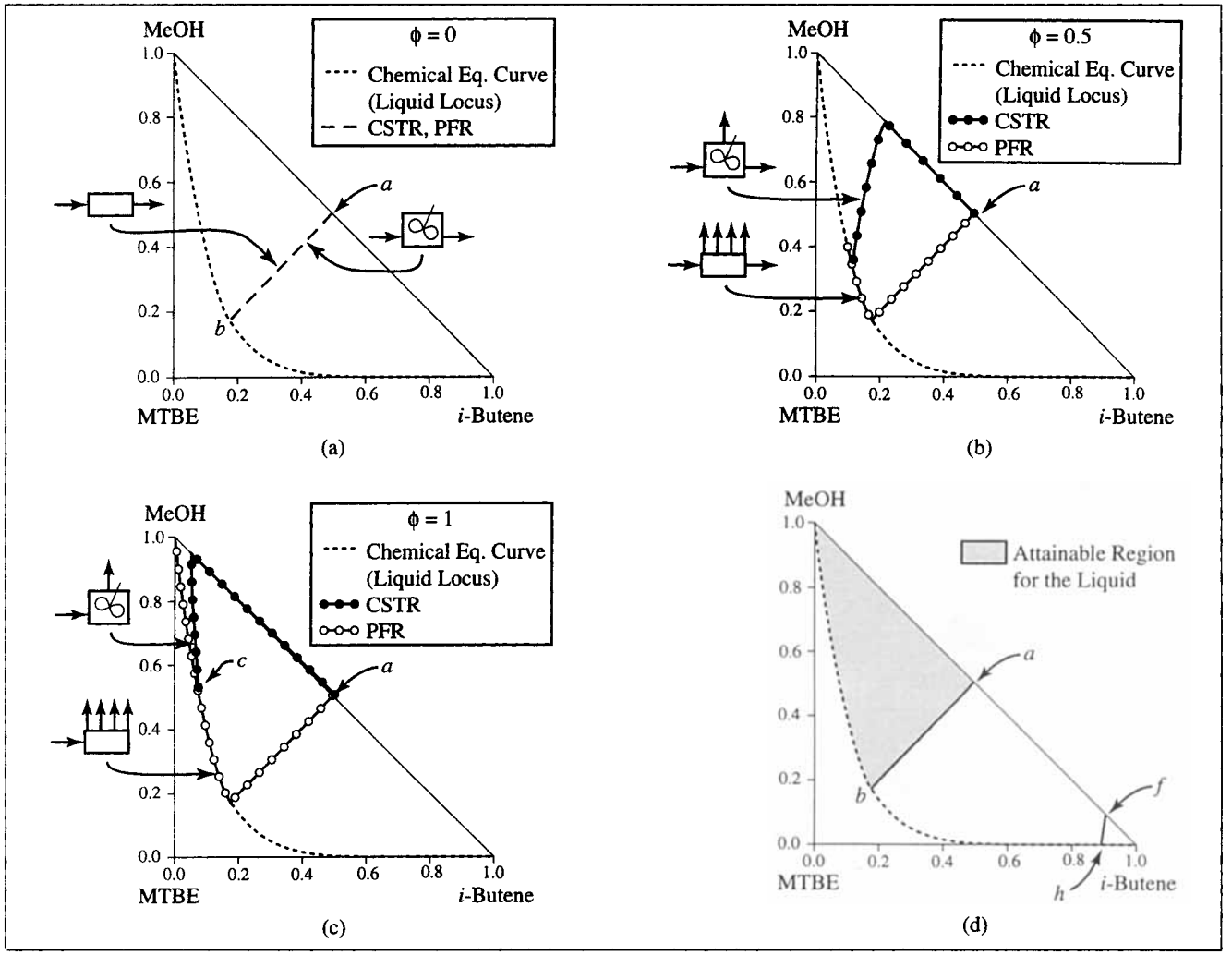


**Figure 8. MTBE system at 8 atm: reactor compositions and attainable region for the liquid.**

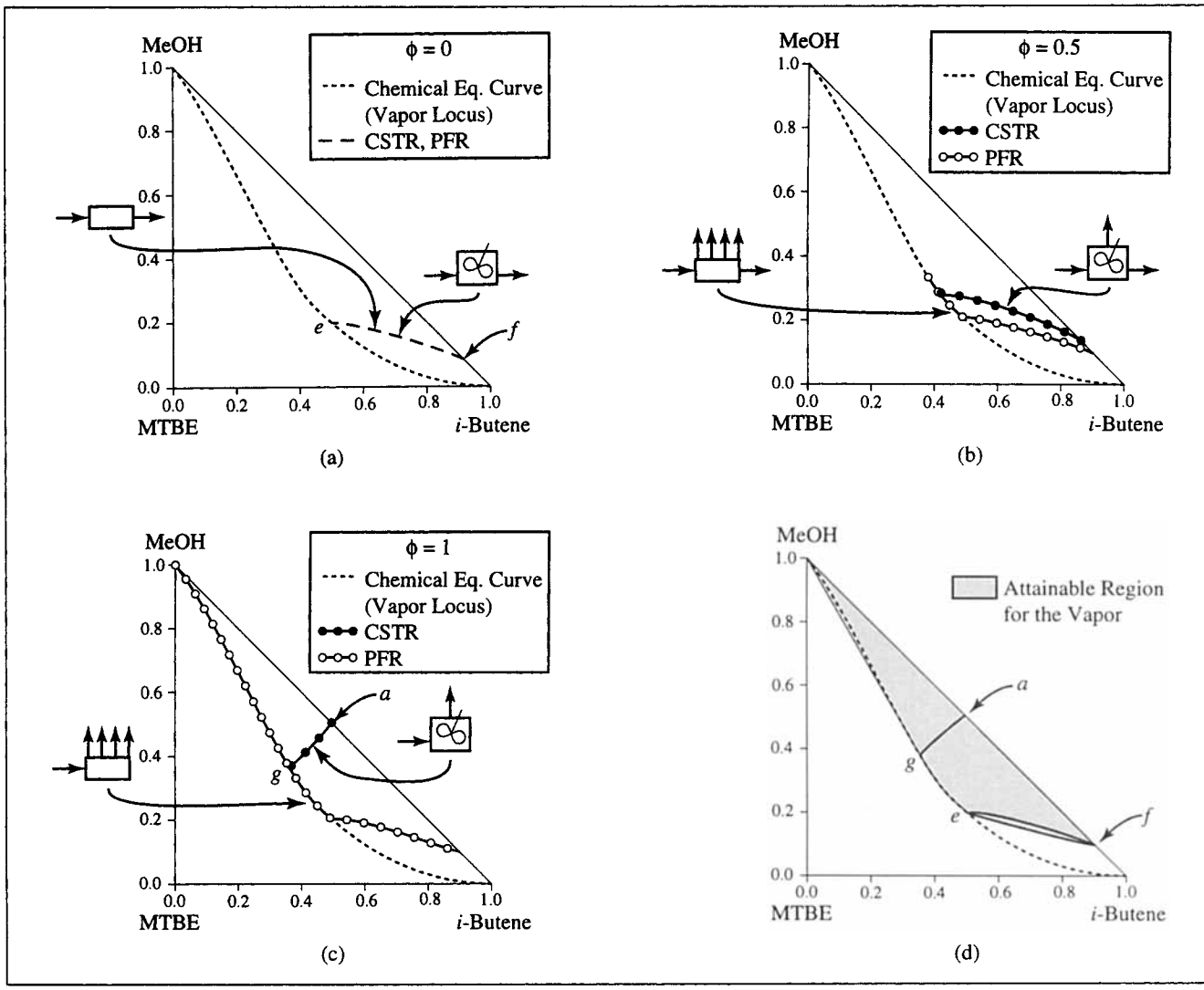


**Figure 9. MTBE system at 8 atm: reactor compositions and attainable region for the vapor.**

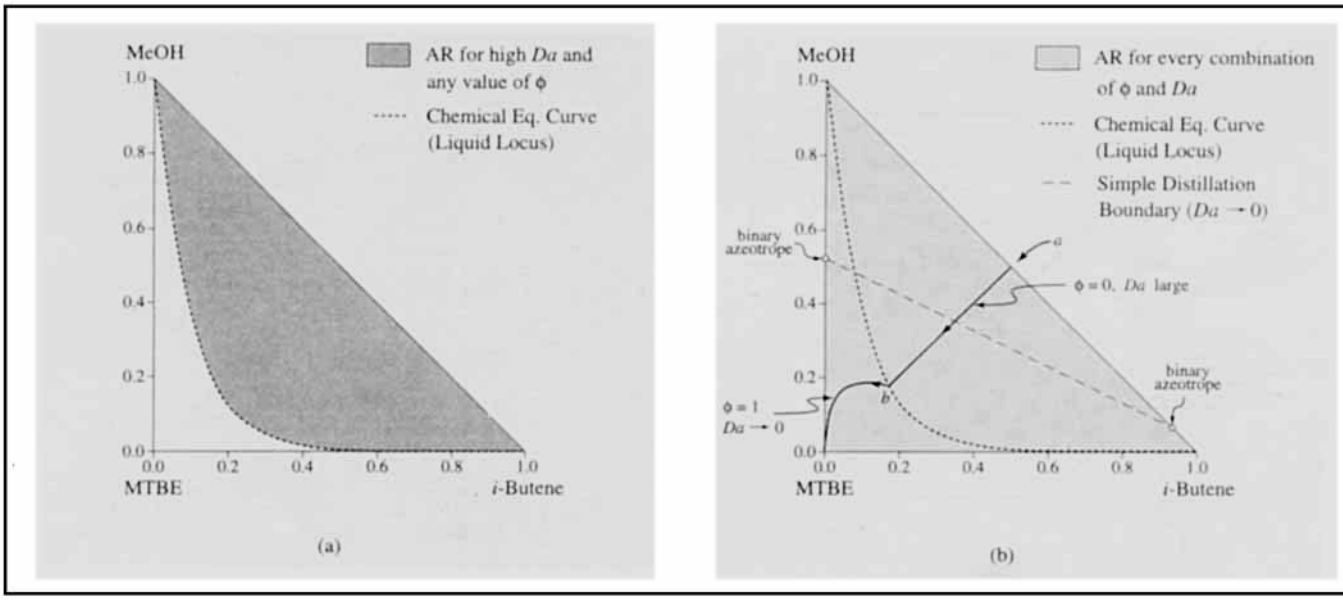


**Figure 10. Attainable regions for the MTBE system: (a) high *Da* and any value of $\phi$; (b) all values of *Da* and $\phi$.**

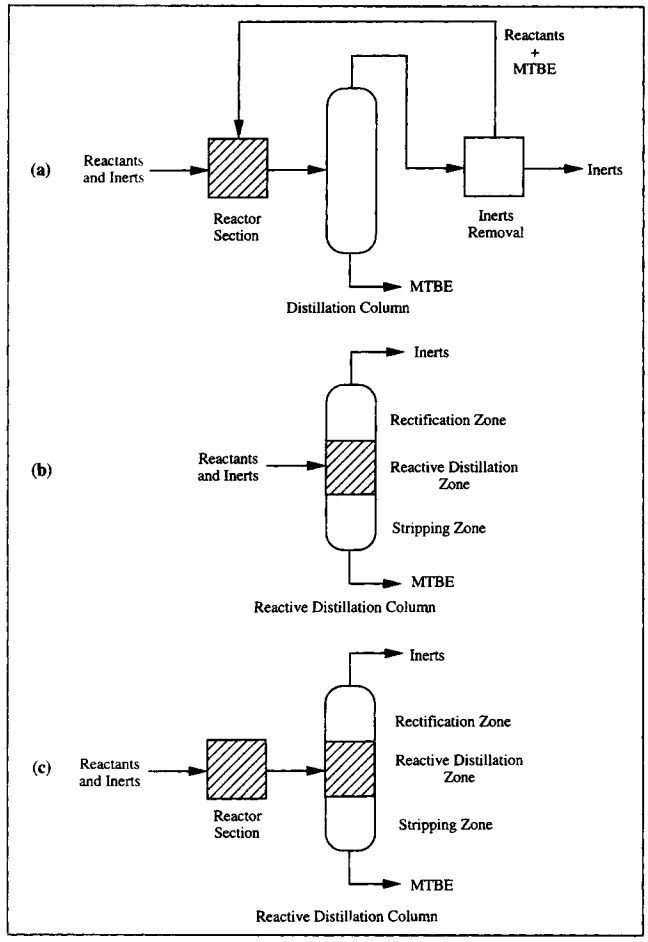


**Figure 11. Flowsheet alternatives for the MTBE process.**

1981, 1990; De Garmo et al., 1992). Sometimes a combination of the two processes is also adopted (Figure 11c).

## Conclusions

We have developed a geometric approach for the feasibility analysis of systems with simultaneous reaction and separation. Reactor–separator models have been derived in mole fraction space for vapor–liquid equilibrium systems in which the chemical reaction occurs in the liquid phase. These models can be described in terms of two independent dimensionless parameters: the Damköhler number, which relates the residence time to the characteristic reaction time, and the vapor fraction $\phi$, which depends on the heating policy.

By introducing the reaction–separation vector is has been shown that the reactor–separator models have the same geometric properties as the simple reactor models in concentration space. Hence, the procedure for constructing the attainable region previously developed (Glasser et al., 1987) can be applied.

The two ternary examples show how the attainable region can be extended when reaction and separation occur simultaneously. By analyzing the features of the PFR trajectories and CSTR loci, we have pointed out the advantages and the limitations of the attainable region. It allows us to identify promising flowsheets in a design procedure. Nevertheless it is a preliminary approach to reactor network synthesis: a cost analysis is still needed to determine which alternative is economically favored.

The method we have shown is not limited to distillation. In fact, we restrict the analysis to distillation only when we introduce the VLE relationship, which relates the vapor composition $y$ to the liquid composition $x$. In principle, $y$ does not have to represent a vapor phase, but it could be, for instance, a composition vector in a second liquid phase. This allows us to use the approach for other two-phase reaction–separation techniques, such as liquid–liquid extraction or membranes, as long as an algebraic relationship between the two composition vectors $x$ and $y$ is known.

## Acknowledgments

We are grateful for the financial support provided by sponsors of the University of Massachusetts Center for Process Design and Control. We are also grateful to Ganesh Venimadhavan for helpful discussions and Ms. Pam Stephan for drawing some of the figures.

## Notation

$F$ = inlet liquid molar flow rate, mol/s
$F_m$ = inlet liquid mass flow rate, kg/s
$k_f$ = forward reaction-rate constant, 1/s
$L_m$ = outlet liquid mass flow rate, kg/s
$M_i$ = molecular weight of component $i$, g/mol
$N_C$ = number of components
$N_R$ = number of CSTR in series
$P$ = total pressure, Pa
$P_i^{sat}$ = saturated vapor pressure of component $i$, Pa
$R$ = reaction-separation vector
$V$ = vapor molar flow rate, mol/s
$V_m$ = vapor mass flow rate, kg/s
$x_i$ = mole fraction of component $i$ in the liquid phase
$y_i$ = mole fraction of component $i$ in the vapor phase
0 = initial value (subscript)

### *Greek letters*

$\delta$ = value of $Da_j$ in the series of CSTRs
$\bullet$ = value of $\phi_j$ in the series of CSTRs
$\zeta$ = dimensionless time variable
$\eta$ = "warped" dimensionless time variable
$\gamma_i$ = activity coefficient of component $i$
$\nu$ = vector of the stoichiometric coefficients
$\rho_m$ = mass density of the liquid phase, kg/m$^3$
$\tau$ = residence time, s
$\phi_j$ = vapor fraction for the $j$th reactor in the series of CSTRs

## Literature Cited

Al-Jarallah, A. M., M. A. B. Siddiqui, and A. K. K. Lee, "Kinetics of Methyl Tertiary Butyl Ether Synthesis Catalyzed by Sulfuric Acid," *Chem. Eng. J.*, **39**, 169 (1988).

Aris, R., "Studies in Optimization: I. The Optimum Design of Adiabatic Reactors with Several Beds," *Chem. Eng. Sci.*, **12**, 243 (1960a).

Aris, R., "Studies in Optimization: II. Optimum Temperature Gradients in Tubular Reactors," *Chem. Eng. Sci.*, **13**, 18 (1960b).

Aris, R., "Studies in Optimization: III. The Optimum Operating Conditions in Sequences of Stirred Tank Reactors," *Chem. Eng. Sci.*, **13**, 75 (1960c).

Aris, R., "Studies in Optimization: IV. The Optimum Conditions for a Single Reaction," *Chem. Eng. Sci.*, **13**, 197 (1961).

Balakrishna, S., and L. T. Biegler, "A Unified Approach for the Simultaneous Synthesis of Reaction, Energy, and Separation Systems," *Ind. Eng. Chem. Res.*, **32**, 1372 (1993).

Brake, L. D., "Preparation of Dimethyl Ether by Catalytic Dehydration of Methanol," U.S. Patent No. 4,595,785 (June 17, 1986).

De Garmo, J. L., V. N. Parulekar, and V. Pinjala, "Consider Reactive Distillation," *Chem. Eng. Prog.*, **88**, 43 (1992).
Espinosa, J., P. Aguirre, and G. A. Perez, "Product Composition Regions of Single-Feed Reactive Distillation Columns: Mixtures Containing Inerts," *Ind. Eng. Chem. Res.*, **34**, 853 (1995).
Feinberg, M., and D. Hildebrandt, "Optimal Reactor Design from a Geometric Viewpoint: I. Universal Properties of the Attainable Region," *Chem. Eng. Sci.*, submitted (1996).
Fidkowski, Z. T., M. F. Doherty, and M. F. Malone, "Feasibiity of Separations for Distillation of Nonideal Ternary Mixtures," *AIChE J.*, **39** 1303 (1993).
Foucher, E., M. F. Malone, and M. F. Doherty, "Automatic Screening of Entrainers in Homogeneous Azeotropic Distillation," *Ind. Eng. Chem. Res.*, **30**, 760 (1991).
Glasser, D., D. Hildebrandt, and C. Crowe, "A Geometric Approach to Steady Flow Reactors: The Attainable Region and Optimization in Concentration Space," *Ind. Eng. Chem. Res.*, **26**, 1803 (1987).
Glasser, B., D. Hildebrandt, and D. Glasser, "Optimal Mixing for Exothermic Reversible Reactions," *Ind. Eng. Chem. Res.*, **31**, 1541 (1992).
Glasser, D., D. Hildebrandt, and S. Godorr, "The Attainable Region for Segregated, Maximum Mixed, and Other Reactor Models," *Ind. Eng. Chem. Res.*, **33**, 1136 (1994).
Godorr, S. A., D. Hildebrandt, and D. Glasser, "The Attainable Region for Systems with Mixing and Multiple-rate Processes: Finding Optimal Reactor Structures," *Chem. Eng. J.*, **54**, 175 (1994).
Hildebrandt, D., and D. Glasser, "The Attainable Region and Optimal Reactor Structures," *Chem. Eng. Sci.*, **45**, 2161 (1990).
Hildebrandt, D., D. Glasser, and C. Crowe, "Geometry of the Attainable Region Generated by Reaction and Mixing: With and Without Constraints," *Ind. Eng. Chem. Res.*, **29**, 49 (1990).
Horn, F., "Attainable and Non-Attainable Regions in Chemical Reaction Technique," *Euro. Symp. on Chemical Reaction Engineering*, Pergamon Press, New York, p. 293, (1964).
Jaswal, I., C. Cliff, and K. Pugi, "Preparation of Polyamides by Continuous Polymerization," U.S. Patent No. 3,900,450 (Aug. 19, 1975).
Jobson, M., D. Hildebrandt, and D. Glasser, "Attainable Products for the Vapour-Liquid Separation of Homogeneous Ternary Mixtures," *Chem. Eng. J.*, **59**, 51 (1995).
Kokossis, A. C., and C. A. Floudas, "Optimization of Complex Reactor Networks—I. Isothermal Operation," *Chem. Eng. Sci.*, **45**, 595 (1990).
Kokossis, A. C., and C. A. Floudas, "Optimization of Complex Reactor Networks—II. Nonisothermal Operation," *Chem. Eng. Sci.*, **49**, 1037 (1994).
Modell, M., and R. C. Reid, *Thermodynamics and Its Applications*, 2nd ed., Prentice Hall, Englewood Cliffs," NJ, p. 331 (1983).
Omtveit, T., J. Tanskanen, and K. Lien, "Graphical Targeting Procedures for Reactor Systems," *Comp. Chem. Eng.*, **18**, S113 (1994).
Pinney, B. M., "Regulating the Flow of Molten Polyamides in a Continuous Process for the Preparation Thereof," U.S. Patent No. 3,960,820 (June 1, 1976).
Prausnitz, J. M., T. F. Anderson, E. A. Grens, C. A. Eckert, R. Hsieh, and J. P. O'Connell, *Computer Calculations for Multicomponent Vapor-Liquid and Liquid-Liquid Equilibria*, Prentice Hall, Englewood Cliffs, NJ, p. 58 (1980).
Rehfinger, A., and U. Hoffmann, "Kinetics of Methyl Tertiary Butyl Ether Liquid Phase Synthesis Catalyzed by Ion Exchange Resin: I. Intrinsic Rate Expression in Liquid Phase Activities," *Chem. Eng. Sci.*, **45**, 1605 (1990).
Reid, R. C., J. M. Prausnitz, and B. E. Poling, *The Properties of Gases and Liquids*, 4th ed., McGraw-Hill, New York (1987).
Shinnar, R., and C. A. Feng, "Structure of Complex Catalytic Reactions: Thermodynamic Constraints in Kinetic Modeling and Catalyst Evaluation," *Ind. Eng. Chem. Fundam.*, **24**, 153 (1985).
Smith, L. A., "Catalytic Distillation Process," U.S. Patent No. 4,307, 254 (Dec. 22, 1981).
Smith, L. A., "Method for the Preparation of Methyl Tertiary Butyl Ether," U.S. Patent No. 4,978,807 (Dec. 18, 1990).
Steppan, D. D., M. F. Doherty, and M. F. Malone, "A Flowing Film Model for Continuous Nylon 6,6 Polymerization," *Ind. Eng. Chem. Res.*, **28**, 1324 (1989).
Steppan, D. D., M. F. Doherty, and M. F. Malone, "Wiped Film Reactor Model for Nylon 6,6 Polymerization," *Ind. Eng. Chem. Res.*, **29**, 2012 (1990).
Sundmacher, K., and U. Hoffmann, "Macrokinetic Analysis of MTBE-Synthesis in Chemical Poetentials," *Chem. Eng. Sci.*, **49**, 3077 (1994).
Taylor, G. B., "Process for Making Polyamides," U.S. Patent No. 2,361,717 (Oct. 31, 1944).
Ung, S., and M. F. Doherty, "Necessary and Sufficient Conditions for Reactive Azeotropes in Multireaction Mixtures," *AIChE J.*, **41**, 2383 (1995a).
Ung, S., and M. F. Doherty, "Vapor-Liquid Phase Equilibrium in Systems with Multiple Chemical Reactions," *Chem. Eng. Sci.*, **50**, 23 (1995b).
Ung, S., and M. F. Doherty, "Theory of Phase Equilibria in Multireaction Systems," *Chem. Eng. Sci.*, **50**, 3201 (1995c).
Ung, S., and M. F. Doherty, "Calculation of Residue Curve Maps for Mixtures with Multiple Equilibrium Chemical Reactions," *Ind. Eng. Chem. Res.*, **34**, 3195 (1995d).
Venimadhavan, G., G. Buzad, M. F. Doherty, and M. F. Malone, "Effect of Kinetics on Residue Curve Maps for Reactive Distillation," *AIChE J.*, **40**, 1814 (1994).
Wahnschafft, O. M., J. W. Koehler, E. Blass, and A. W. Westerberg, "The Product Composition Regions for Single-Feed Azeotropic Distillation Columns," *Ind. Eng. Chem. Res.*, **31**, 2345 (1992).

## Appendix: Stopping Criteria for the PFR Model

Since the independent variables $\zeta$ and $\eta$ in Eqs. 18 and 22 are related to the Damköhler number, once $Da$ is specified, the final value of the independent variable becomes determined. It is possible to find an analytical expression for $\zeta_{\text{exit}}$ as a function of $Da$. Equation 19 is equivalent to

$$\frac{d\zeta}{dz} = \frac{k_{f,\min}\,\rho_m A}{L_m}. \tag{A1}$$

In the limit $N_R \to \infty$, we have

$$\lim_{N_R \to \infty} \frac{\epsilon}{\delta} = \frac{\bar{V}_m}{k_{f,\min}\,\rho_m A} = \frac{\phi}{Da}. \tag{A2}$$

Therefore Eq. A1 can be rewritten as

$$\frac{d\zeta}{dz} = \frac{Da}{\phi}\frac{\bar{V}_m}{L_m}. \tag{A3}$$

The overall material balance in mass quantities is

$$\frac{dL_m}{dz} = -\bar{V}_m. \tag{A4}$$

By substituting Eq. A4 in Eq. A3 and eliminating $dz$, we can obtain

$$d\zeta = -\frac{Da}{\phi}\, d\ln L_m, \tag{A5}$$

which integrated with the initial condition $L_m(0) = F_m$ gives

$$\zeta = \frac{Da}{\phi}\ln\frac{F_m}{L_m}. \tag{A6}$$

Since $L_m = F_m(1-\phi)$ at the exit of the reactor, we can calculate $\zeta_{\text{exit}}$:

$$\zeta_{exit} = \frac{Da}{\phi} \ln \frac{1}{1-\phi}. \tag{A7}$$

When $\phi \to 0$ (no vaporization takes place) $\zeta_{exit} \to Da$. When $\phi \to 1$ (all the feed is vaporized) $\zeta_{exit} \to \infty$.

If $\eta$ is the independent variable, $\eta_{exit}$ cannot be determined anlaytically, but it can still be found numerically. From Eq. (A5), by taking into account the relationship between $d\eta$ and $d\zeta$ (Eq. 23), we get

$$d\eta = -\frac{Da}{\phi} \frac{M(x)}{M(x_0)} d\ln L_m, \tag{A8}$$

which can be rearranged as

$$\frac{dL_m}{d\eta} = -\frac{\phi}{Da} \frac{M(x_0)}{M(x)} L_m. \tag{A9}$$

With the initial condition $L_m(0) = F_m$, Eq. A.9 is coupled with the system of ODEs defined by Eq. 22. The quantity $\eta_{exit}$ corresponds to the value of $\eta$ for which $L_m = F_m(1-\phi)$.

*Manuscript received June 17, 1996.*